BIOCHEMISTRY
including biophysical chemistry & molecular biology

Article

pubs.acs.org/biochemistry

Oxy Intermediates of Homoprotocatechuate 2,3-Dioxygenase: Facile Electron Transfer between Substrates

Michael M. Mbughuni,[†,§] Mrinmoy Chakrabarti,[∥] Joshua A. Hayden,[∥] Katlyn K. Meier,[∥] Joseph J. Dalluge,[‡] Michael P. Hendrich,*[,∥] Eckard Münck,*[,∥] and John D. Lipscomb*[,†,§]

[†]Department of Biochemistry, Molecular Biology and Biophysics, [‡]Department of Chemistry, and [§]Center for Metals in Biocatalysis, University of Minnesota, Minneapolis, Minnesota 55455, United States

[∥]Department of Chemistry, Carnegie Mellon University, Pittsburgh, Pennsylvania 15213, United States

Supporting Information

ABSTRACT: Substrates homoprotocatechuate (HPCA) and O_2 bind to the Fe^{II} of homoprotocatechuate 2,3-dioxygenase (FeHPCD) in adjacent coordination sites. Transfer of an electron(s) from HPCA to O_2 via the iron is proposed to activate the substrates for reaction with each other to initiate aromatic ring cleavage. Here, rapid-freeze-quench methods are used to trap and spectroscopically characterize intermediates in the reactions of the HPCA complexes of FeHPCD and the variant His200Asn (FeHPCD−HPCA and H200N−HPCA, respectively) with O_2. A blue intermediate forms within 20 ms of mixing of O_2 with H200N−HPCA ($H200N^{HPCA}_{Int1}$). Parallel mode electron paramagnetic resonance and Mössbauer spectroscopies show that this intermediate contains high-spin Fe^{III} ($S = {}^5/_2$) antiferromagnetically coupled to a radical ($S_R = {}^1/_2$) to yield an $S = 2$ state. Together, optical and Mössbauer spectra of the intermediate support assignment of the radical as an HPCA semiquinone, implying that oxygen is bound as a (hydro)peroxo ligand. $H200N^{HPCA}_{Int1}$ decays over the next 2 s, possibly through an Fe^{II} intermediate ($H200N^{HPCA}_{Int2}$), to yield the product and the resting Fe^{II} enzyme. Reaction of FeHPCD−HPCA with O_2 results in rapid formation of a colorless Fe^{II} intermediate ($FeHPCD^{HPCA}_{Int1}$). This species decays within 1 s to yield the product and the resting enzyme. The absence of a chromophore from a semiquinone or evidence of a spin-coupled species in $FeHPCD^{HPCA}_{Int1}$ suggests it is an intermediate occurring after O_2 activation and attack. The similar Mössbauer parameters for $FeHPCD^{HPCA}_{Int1}$ and $H200N^{HPCA}_{Int2}$ suggest these are similar intermediates. The results show that transfer of an electron from the substrate to the O_2 via the iron does occur, leading to aromatic ring cleavage.

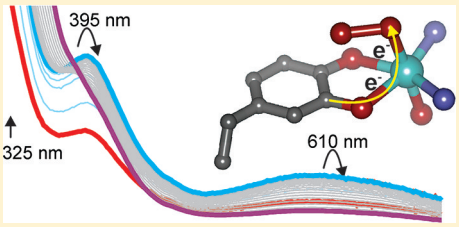

Extradiol dioxygenases make up a class of nonheme Fe^{II} (or occasionally Mn^{II})-containing enzymes that catalyze the cleavage of catecholic substrates adjacent to the vicinal OH functions with incorporation of both atoms of oxygen from O_2 (Scheme 1).[1−5] This reaction allows a host of aerobic microorganisms to channel carbon from naturally occurring and man-made aromatic compounds into the TCA cycle, facilitating biodegradation.[1,4,6,7] As such, the catechol ring-cleaving dioxygenases have roles in human health and maintenance of the global carbon cycle.

Extradiol dioxygenases were the first members of the large class of so-called 2-His-1-carboxylate facial triad enzymes to be recognized.[8] Members of this enzyme class utilize two His residues and one Asp/Glu residue to bind the divalent metal through one face of the coordination surface, leaving the other face free to bind solvents or reaction substrates.[9,10] Often a substrate or cofactor will bind to, or very close to, the metal, causing release of the solvents and opening a coordination site for O_2 (see ref 11 for examples). It has been shown that, in the case of the extradiol dioxygenases, the catecholic substrates and O_2 bind to the metal in adjacent coordination sites (Scheme 1A−D).[12] We and others have proposed that transfer of an electron from the substrate to the oxygen via the metal gives radical character to both the substrate and the oxygen (Scheme 1B−D).[1,10,12−14] Recombination of the radicals to form a metal-bound alkylperoxo intermediate would initiate aromatic ring cleavage (Scheme 1E−G).

An oxygen activation mechanism of this type does not require a formal change in oxidation state of the metal between the initial enzyme−aromatic substrate complex and postulated diradical reactive state (Scheme 1D). Accordingly, it has recently been shown that the recombinant extradiol dioxygenase homoprotocatechuate 2,3-dioxygenase originally isolated from *Brevibacterium fuscum* [FeHPCD (Scheme 1)] functions with the same k_{cat}, and k_{cat}/K_{mO_2} values within error when the Fe^{II} is replaced with Mn^{II} (MnHPCD).[15] It exhibits even higher k_{cat} and K_{mO_2} values when Co^{II} is substituted.[16] The fact that the enzyme is fully functional using metals with a redox potential range spanning 1.15 V suggests either no change in metal oxidation state or no net change between the enzyme form that can bind O_2 and that which can irreversibly attack the substrate. An indication that the metal transiently changes redox state prior to formation of the reactive species has come from a

Received: September 14, 2011
Revised: October 18, 2011
Published: October 20, 2011

Scheme 1. Proposed Reaction Mechanism for Extradiol Dioxygenases[a]

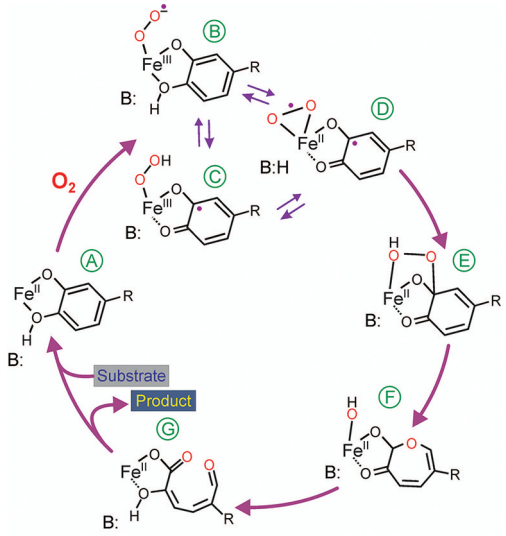

[a]For these studies, R is either CH_2COO^- (HPCA) or NO_2 (4NC). In the case of 4NC, the substrate is fully deprotonated, so the proton required for catalysis must be derived from solvent.

kinetic study of the reaction of MnHPCD with the natural substrate (HPCA) and O_2.[17] A species best described as $Mn^{III}-O_2^{\bullet-}$ is formed in low yield and then decays to a Mn^{II} species within 30 ms of the start of the reaction. This second intermediate may be the alkylperoxo intermediate of the reaction cycle, which then decays to yield the ring-cleaved product.

Investigation of the native FeHPCD mechanism has been facilitated by discovery of methods to slow the rates of steps in the reaction cycle. One method has been to conduct the reaction in a single crystal using the slowly cleaved substrate, 4-nitrocatechol (4NC). It was found that the postulated 4NC–semiquinone ($SQ^{\bullet}$)–$Fe^{II}-O_2^{\bullet-}$ (Scheme 1D) and Fe^{II}–alkylperoxo (Scheme 1E) intermediates, as well as the ring-cleaved product intermediate (Scheme 1G), were stabilized in different active sites of the asymmetric unit of the crystal.[12] This allowed them to be structurally characterized. Another approach to slow the reaction was to use active site variants of the postulated active site acid/base catalyst His200.[18,19] It was found when His200 was replaced with Asn (H200N), and 4NC was used as the substrate, O_2 bound to form a long-lived, antiferromagnetically coupled $Fe^{III}-O_2^{\bullet-}$ species ($H200N^{4NC}_{Int1}$). This species decayed during the following 100 s to another intermediate ($H200N^{4NC}_{Int2}$) postulated to be a 4NC–$SQ^{\bullet}$–Fe^{III}–peroxo species. Rather than undergoing ring cleavage, this intermediate decayed to release 4NC quinone and H_2O_2 and restore the Fe^{II} center of the enzyme. This study showed that a change in the iron redox state can occur as O_2 binds, but the downstream chemistry deviates from normal catalysis, suggesting that the H200N mutation and/or the use of a substrate with an electron-withdrawing substituent can uncouple O_2 activation from ring cleavage chemistry.

Transient kinetic studies of extradiol dioxygenase reactions that yield the correct ring-cleaved products have been conducted using HPCA as the substrate for FeHPCD and H200N.[18,20] These studies revealed at least four intermediates following addition of O_2 with a preformed enzyme–substrate complex. In the case of H200N, the O_2 binding step itself could be monitored because a visible absorption band associated with the complex was observed near 610 nm.

In this study, we use rapid-freeze-quench (RFQ) methods to trap and spectroscopically characterize the intermediates from the reaction of FeHPCD– and H200N–HPCA complexes with O_2. The earliest trapped intermediates differ markedly from that identified in the reaction of H200N–4NC with O_2.[19] Together, they support a mechanism in which facile transfer of an electron between bound HPCA and O_2 via the Fe^{II} forms the basis for O_2 activation and insertion chemistry.

EXPERIMENTAL PROCEDURES

Reagents and Enzymes. All chemicals were purchased from Sigma-Aldrich and were used without purification except for HPCA, which was recrystallized from water at 4 °C to remove minor contaminants. Anaerobic conditions were achieved by repeated cycling of solutions between argon gas and vacuum. We removed trace contaminating O_2 from the Ar gas by passing it through an Agilent GC-1 POP O_2 scrubbing cartridge and then through an Agilent GC-4 POP O_2 indicating cartridge. Formate dehydrogenase (FDH) was prepared as previously described.[21] The C_1 and C_2 *p*-hydroxyphenylacetate hydroxylase system from *Acinetobacter baumannii* was a generous gift from D. P. Ballou. Recombinant *B. fuscum* FeHPCD and the H200N variant were expressed and purified as previously described.[18,22] ^{57}Fe-enriched enzyme was prepared for RFQ/Mössbauer experiments as previously described.[19] Mushroom tyrosinase was purchased from Sigma.

Stopped Flow and Spectroscopy. All stopped-flow experiments were performed using an Applied Photophysics model SX.18MV stopped-flow device at 4 °C. The reaction procedures were as previously described.[20] The kinetic data were analyzed to extract reciprocal relaxation times using Applied Photophysics Pro-Data Viewer version 4.0.17. Electron paramagnetic resonance (EPR) spectra were recorded using a Bruker Elexsys E-500 or Bruker ESP 300 spectrometer each equipped with a Bruker dual mode cavity and an Oxford ESR 910 liquid helium cryostat. Mössbauer spectroscopy was performed as previously described.[19,23] Spectra were analyzed using WMOSS (SEE Co., Edina, MN).

RFQ Methods. Anaerobic substrate complexes were prepared in a Coy glovebox as previously described.[19] RFQ syringes were loaded inside the anaerobic glovebox before they were transferred to the Update RFQ Instrument (model 1019 RFQ) where they were equilibrated at 4 °C for 30 min using an ice bath. After being rapidly mixed and passed through a calibrated delay line, samples were collected by rapid freezing on counter-rotating aluminum wheels at liquid N_2 temperature. A programmed delay was used for time points of >0.4 s. For samples at times of >1.5 s, the mixed sample was collected directly in an EPR tube or Mössbauer cup and frozen by rapid emersion in a dry ice/methanol bath (EPR) or liquid N_2 (Mössbauer) after the appropriate incubation time. We have observed that freezing on the counter-rotating wheels introduces a small splash artifact that becomes more prominent at the highest ram drive speeds. The splashed material falls into the liquid N_2 bath directly and freezes more slowly than the material on the wheel, causing the appearance of the spectrum of the product complex in early samples. The rate of product formation for the reactions investigated here is well-known from stopped-flow experiments,[20] and no product complex is expected in the earliest RFQ samples collected.

dx.doi.org/10.1021/bi201436n | *Biochemistry* 2011, 50, 10262–10274

Synthesis of HPCA Enriched with ^{17}O at the C_3 Hydroxyl Functional Group. 3-^{17}OH-HPCA was prepared from *p*-hydroxyphenylacetate (HPA). The C_1 and C_2 hydroxylase from *A. baumannii*[24] was used to catalyze conversion of HPA to 3-(^{17}OH)-4-(^{16}OH)-dihydroxyphenylacetic acid using 70% enriched $^{17}O_2$ (Cambridge Isotopes). A 2 mL reaction mixture was prepared in a 5 mL pear-shaped flask fitted with a three-way valve in the anaerobic glovebox. Concentrations of the reactants were as follows: 10 μM C_1, 20 μM C_2, 20 μM FDH, 100 μM NADH, 15 mM formate, and 10 mM HPA. The flask mouth was capped with a SUBA seal septum crimped with copper wire and the valve closed prior to removal from the glovebox. The three-way valve was connected to a vacuum/argon line and to a tank of 70% enriched $^{17}O_2$, and the lines were evacuated and exchanged with argon several times. The system was opened to vacuum, and the head space of the pear-shaped flask was evacuated for ~1 s. The vacuum line was closed, and the flask was filled with 1−2 psi of 70% enriched $^{17}O_2$ to initiate the reaction. The reaction was allowed to proceed for 2 h at room temperature to reach completion and then quenched with 3% H_2SO_4. The quenched reaction mixture was centrifuged at 39000*g* for 40 min to remove insoluble materials. The supernatant from centrifugation was assayed for HPCA using the catalytic activity of FeHPCD, which converts HPCA to the α-hydroxy δ-carboxymethyl *cis*-muconic semialdehyde, which has an extinction coefficient at 380 nm of 38000 M^{-1} cm^{-1}.[20] The assay revealed nearly stoichiometric conversion of HPA to HPCA. The reaction supernatant containing 3-^{17}OH-HPCA was lyophilized, dissolved in 50 mM MOPS buffer (pH 7.5), and stored at −80 °C until it was used in RFQ experiments. LC−MS/MS analysis of the synthesized HPCA is described in the Supporting Information and shows nearly 68% enrichment of one atom of ^{17}O per HPCA molecule.

Preparation of HPCA Quinone. HPCA was oxidized using mushroom tyrosinase (Sigma) in 100 mM MES buffer (pH 5.6) at 4 °C. The reaction was initiated and monitored using the stopped-flow spectrometer with diode array detection. A solution of 2 mM HPCA was mixed with 10 mg/mL mushroom tyrosinase. The quinone product formed during the first 5 min of the reaction and then slowly decayed to an unidentified secondary species.

RESULTS

Single-Turnover Studies of the H200N−HPCA + O_2 Reaction Reveal a Transient Intermediate. Our previous stopped-flow studies revealed the accumulation of at least four reaction cycle intermediates after the preformed H200N−HPCA complex reacts with O_2 in a single-turnover reaction.[18] Improvements in the stopped-flow instrumentation and procedures[19] allow the first of these intermediates to accumulate at higher yields so that it can be studied in detail.

As shown in Figure 1A, for the reaction of a stoichiometric (per active site) H200N−HPCA complex with a slight excess of O_2 at pH 7.5, the previously described 610 nm transient intermediate ($H200N^{HPCA}_{Int1}$; ε_{610} ~ 1100 M^{-1} cm^{-1}) rapidly accumulates and then more slowly decays to give the ring-cleaved product (ε_{380} ~ 38000 M^{-1} cm^{-1}). The absorption maximum for product is shifted to 325 nm (ε_{325} ~ 23600 M^{-1} cm^{-1}) when the reaction is conducted at pH 5.5, allowing a second maximum in the spectrum of $H200N^{HPCA}_{Int1}$ to be observed near 395 nm (ε_{395} ~ 3200 M^{-1} cm^{-1}) (Figure 1B). These same features and an additional feature at 310 nm are

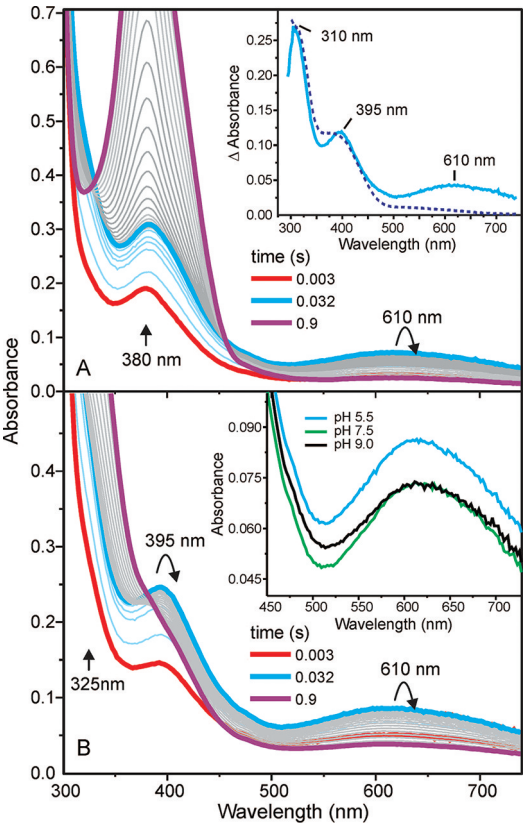

Figure 1. H200N−HPCA + O_2 reaction monitored by stopped-flow methods. (A) Diode array spectra recorded between 3 ms and 2 s after stoichiometric 640 μM (sites) H200N−HPCA anaerobic complex had been mixed with O_2-saturated buffer (~1.8 mM) (1:1) at 4 °C in 200 mM MOPS (pH 7.5) (2 mm path length). The thick line spectra are for the specific times shown. The thin cyan line is for 3−32 ms, and the gray line for 32 ms to 2 s. The inset shows a spectrum that results from subtraction of the spectrum at 3 ms from that at 32 ms (cyan) and the spectrum of HPCA quinone produced by treatment of HPCA with mushroom tyrosinase (blue, dashed). (B) Time courses of the same reaction as in panel A, but in 200 mM MES buffer (pH 5.5). The inset shows a comparison of the spectra of the 610 nm feature formed at pH 5.5, 7.5, and 9.0.

revealed by subtracting the 3 ms spectrum from the 32 ms spectrum for the reaction at pH 7.5 (Figure 1A, inset). When the reaction is conducted at pseudo-first-order concentrations of O_2 at pH 7.5 (Figure S1 of the Supporting Information), the time course can be fit well by a two-sum exponential equation with reciprocal relaxation times ($1/\tau_1$ = 230 ± 20 s^{-1}, and $1/\tau_2$ = 1.6 ± 0.2 s^{-1}) showing that the reaction consists of at least two steps. The spectroscopic data reported below show that the intermediate builds to a nearly stoichiometric yield. The observed value of $1/\tau_1$ is linearly dependent on O_2 concentration with a zero intercept,[18] suggesting that the reaction is irreversible O_2 binding for which $1/\tau_1 = k_{form} = k_1$. The formation of the alkylperoxo intermediate and the ring-cleaving reaction are also likely to be irreversible so that $1/\tau_2 = k_{decay} = k_2$ for $H200N^{HPCA}_{Int1}$. At pH 5.5, the reaction is slightly slower because of a decrease in k_2 (k_1 = 240 ± 20 s^{-1}, and k_2 = 1.1 ± 0.1 s^{-1}). The two reciprocal relaxation times derived from the fits of the time course at this pH are found to be independent of wavelength when monitored at 310, 395, or 610 nm, suggesting that all features result from $H200N^{HPCA}_{Int1}$. The spectra of the intermediate change very little in the range

dx.doi.org/10.1021/bi201436n | *Biochemistry* 2011, 50, 10262−10274

between pH 5.5 and 9 (Figure 1B, inset). The reaction could not be monitored at pH values significantly above pH 9 because of structural alterations of the enzyme.

RFQ EPR and Mössbauer Studies Show That $H200N^{HPCA}_{Int1}$ Has an $S_1 = {}^5/_2$ Fe^{III} Site Coupled to an $S_R = {}^1/_2$ Radical. The anaerobic H200N–HPCA complexes (see below) contain a high-spin Fe^{II} that is EPR-silent in both perpendicular (not shown) and parallel modes (Figure 2, top).

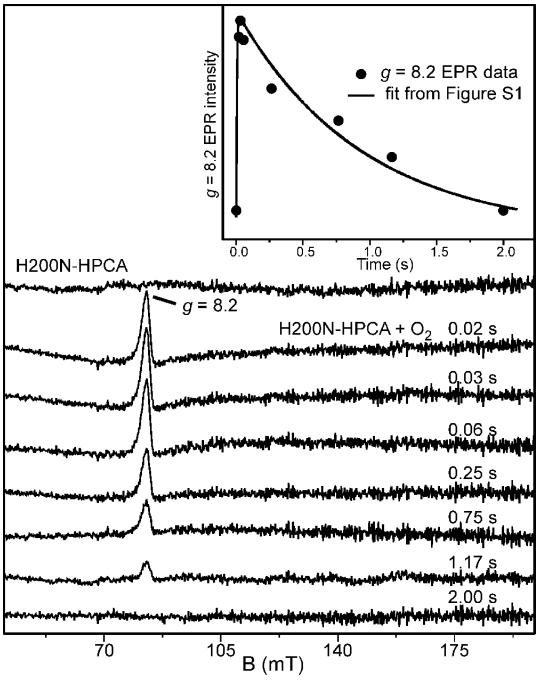

Figure 2. Time-dependent parallel mode EPR spectra from the H200N–HPCA + O_2 reaction. Parallel mode EPR spectra in the $g = 8$ region of RFQ samples frozen between 0 (top, unreacted) and 2 s after 1.65 mM anaerobic H200N–HPCA complex had been mixed with O_2-saturated buffer (1:1) at 4 °C in 200 mM MOPS buffer (pH 7.5) are shown. EPR conditions: frequency, 9.35 GHz; microwave power, 50.4 mW; modulation amplitude, 1 mT; and temperature, 50 K. The inset shows the time course of the $g = 8.2$ signal intensity (●). The solid line is the fit to the optically monitored time course at 610 nm from Figure S1 of the Supporting Information.

The parallel mode EPR spectra of RFQ samples frozen at times between 20 ms and 2 s during the time course of the reaction of this complex with O_2 are shown in Figure 2. At 20 ms, an EPR resonance near $g = 8.2$ is observed in parallel mode (Figure 2). This feature is maximal at approximately 40 ms and then decays over the course of 2 s.

A superposition of the fit of the 610 nm stopped-flow data from Figure S1 of the Supporting Information and the $g = 8.2$ EPR time course is shown in the inset of Figure 2. The congruence of these data indicates that the $g = 8.2$ EPR feature originates from $H200N^{HPCA}_{Int1}$. Furthermore, the observation of this signal in parallel mode and its absence in perpendicular mode demonstrate that it belongs to a species with an integer electronic spin.

The EPR spectrum of $H200N^{HPCA}_{Int1}$ quenched at 40 ms is shown in more detail in Figure 3. The spectrum has contributions from two species, namely, $H200N^{HPCA}_{Int1}$ ($g = 8.2$) and a broader resonance from an Fe^{II} species. At 2 K, the $g = 8.2$ signal intensity is small relative to that of the Fe^{II} species. The $g = 8.2$ feature is significantly larger at 10 K, indicating that

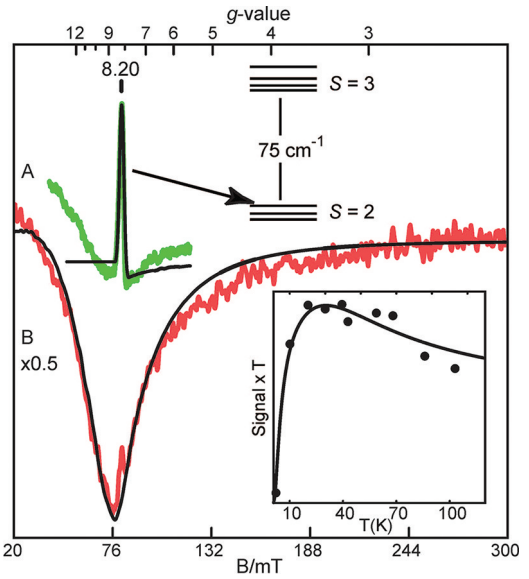

Figure 3. Parallel mode EPR spectra (colored) and simulations (black) for H200N–HPCA frozen 40 ms after reaction with O_2 at (A) 10 and (B) 2 K. Prior to mixing with O_2-saturated buffer: 1.5 mM H200N–HPCA and 200 mM MOPS buffer (pH 7.5). Simulation parameters: (A) $S_1 = {}^5/_2$, $S_R = {}^1/_2$, $J = 25$ cm^{-1}, $D_1 = 1$ cm^{-1}, $E/D_1 = 0.12$, $g_{1z} = 2.015$, and $g_{Rz} = 2.00$ and (B) $S = 2$, $D = -4$ cm^{-1}, $E/D = 0.15$, and $g_z = 2.00$. EPR conditions: microwave, 20 (A) and 0.2 mW (B) at 9.29 GHz; modulation, 1 mT. The intensity of spectrum B has been reduced by a factor of 2. The inset shows a plot of the signal times temperature for the $g = 8.2$ feature and a theoretical fit to this intensity.

it originates from an excited spin doublet. The Mössbauer spectra discussed below reveal that the iron of $H200N^{HPCA}_{Int1}$ is high-spin ($S_1 = {}^5/_2$) Fe^{III} that resides in a complex with an integer spin. The Mössbauer and EPR data are readily reconciled by assuming that $H200N^{HPCA}_{Int1}$ has an $S_1 = {}^5/_2$ site that is antiferromagnetically (AF; $J > 0$) coupled to an $S_R = {}^1/_2$ radical. Exchange coupling separates the electric levels into a ground multiplet for which $S = 2$ and an excited state for which $S = 3$. The $g = 8.2$ signal originates from the $M_S = \pm 2$ doublet, at an energy (E) of ≈5.4 cm^{-1}, of the $S = 2$ multiplet; this doublet is indicated in the level diagram in Figure 3. The electronic levels of the system can be described by the spin Hamiltonian (this is the uncoupled representation):

$$\mathcal{H}_e = J\mathbf{S}_1\cdot\mathbf{S}_\mathbf{R} + D_1[S_{1z}{}^2 - 35/12 + (E/D)_1 (S_{1x}{}^2 - S_{1y}{}^2)] + \beta(\mathbf{S}_1\cdot\mathbf{g}_1 + \mathbf{S}_\mathbf{R}\cdot\mathbf{g}_\mathbf{R})\cdot\mathbf{B} \quad (1)$$

where subscripts 1 and R refer to the Fe^{III} and the radical, respectively. The exchange coupling (J), the zero-field splitting (D and E) of the ferric ion, and electronic Zeeman terms have their common definitions. Throughout this work, we will use isotropic $g_1 = 2.015$ and $g_R = 2.00$ (our data are sensitive to only the z component of the tensors). For describing the broadening of the $g = 8.2$ resonance for ^{17}O-enriched samples, it is advisable (reason given below) to use the $S = 2$ Hamiltonian (the coupled representation).

$$\mathcal{H}_{S=2} = D[S_z{}^2 - 2 + (E/D)(S_x{}^2 - S_y{}^2)] + \beta B_z g_z S_z + S_z A_z{}^{O,c} I_z{}^O \quad (2)$$

The parameters of eq 2 are related to those of eq 1 as follows: $D = (4/3)D_1$, $E/D = (E/D)_1$, and $g_z = (7/6)g_{1z} - (1/6)g_{Rz} \approx$

dx.doi.org/10.1021/bi201436n | Biochemistry 2011, 50, 10262–10274

Table 1. Spin Hamiltonian Parameters for Exchange-Coupled Intermediates from EPR (italics) and Mössbauer Spectroscopy

species	δ (mm/s)	ΔE_Q (mm/s)	η	J (cm^{-1})	D_1 (cm^{-1})	$(E/D)_1$	$A_0/g_n\beta_n$ (T)	A^O (MHz) $^{17}O_2$	A^O (MHz) [^{17}O] HPCA	ref
H200N$_{Int1}^{4NC}$	0.5	−0.33	−3[a]	*6(2)*[a]	−0.59	0.20	−21.4(2)	*180*		19
					−0.48	*0.20*				
H200N$_{Int2}^{4NC}$	0.49	0.87	−7.2	*40(10)*	0.67	0.11	−21.5(2)	<5		19
					0.50	*0.13*				
H200N$_{Int1}^{HPCA}$	0.48(1)	0.95(2)	3[a]	*25(5)*	1.1[b]	0.12	−21.5(2)			this work
					1.1	*0.12*				
H200N$_{Int1}^{HPCA}$ $S = 2$ Hamiltonian[b]	0.48	0.95	3		1.5	0.12	−25.1	*17*	*17*	this work

[a] η values of 3 and −3 imply that the EFG is axial around the x and y axes, respectively. [b] The last row lists the parameters as evaluated for the $S = 2$ multiplet of the coupled system. The full Hamiltonian is given in eq 2. This representation must be used for analysis of the ^{17}O data (an explanation is given in the text). If the radical were on the O_2 moiety, the coupling in the uncoupled representation would be 6 × 17 = 102 MHz, which can be compared with the value of 180 MHz reported for H200N$_{Int1}^{4NC}$.

2.00. The third term in eq 2 describes the hyperfine interaction of the ^{17}O nucleus with its electronic environment, where $A_z^{O,c}$ is expressed in the coupled representation. For the $^{17}O_2$-enriched sample, depending on the bonding, there could be one or two ^{17}O nuclei contributing to the broadening. The spectra are only broadened by the nuclear interaction and do not show resolved splittings; thus, the derived value of $A_z^{O,c}$ assumes one ^{17}O interaction and is an upper limit (two equivalent ^{17}O nuclei would reduce $A_z^{O,c}$ by 25%). The temperature dependence of the $g = 8.2$ H200N$_{Int1}^{HPCA}$ signal in Figure 3 is plotted as the signal times the temperature versus temperature. The signal times temperature is proportional to the population of the EPR active doublet, and a fit to the points based on eq 1 gives an exchange coupling constant J of 25 cm^{-1}. The rise of the signal at low temperatures is due to the increasing population of the $M_S = \pm 2$ level within the $S = 2$ multiplet, whereas its decline at higher temperatures reflects population of the $S = 3$ multiplet. The solid line in Figure 3A shows a SpinCount simulation of the H200N$_{Int1}^{HPCA}$ spectrum using the parameters given in the caption and in Table 1. When $J/D_1 \approx 25$, the system is in the strong coupling limit and consists of two well-separated $S = 2$ and $S = 3$ multiplets. The intensity of the EPR signal (accounting for ≈80% of the iron in the sample) is in approximate agreement with the concentration of the sample; however, because of the somewhat variable packing density of the RFQ sample, this concentration has a 10% uncertainty. Figure 3B shows a simulation of the Fe^{II} species with parameters given in the figure caption. This species accounts for ≈20% of the iron in the sample, and it is not present in the starting Fe^{II} enzyme prior to mixing with substrate and oxygen. Further details of this species are given below.

Panels B–E of Figure 4 show selected Mössbauer spectra from the time course of the H200N–HPCA + O_2 reaction; these spectra were recorded at 4.2 K in the absence of an applied magnetic field ($B = 0$). As reported previously, the iron site of H200N (Figure 4A) exhibits one doublet with a quadrupole splitting ΔE_Q of 3.01 mm/s and an isomer shift δ of 1.24 mm/s; these parameters are typical of high-spin Fe^{II} with octahedral O/N coordination.[19] The anaerobically prepared, stoichiometric H200N–HPCA sample of Figure 4B exhibits two high-spin ferrous species, namely, H200N$_{ES1}^{HPCA}$ (green, 60% of Fe) with a ΔE_Q of 3.45 mm/s and a δ of 1.16 mm/s and H200N$_{ES2}^{HPCA}$ (blue, 40%) with a ΔE_Q of 2.32 mm/s and a δ of 1.20 mm/s (see also Table 2). Samples prepared with a 2-fold excess of substrate or at pH 6 displayed the same species in the same ratio.[a] Within 20 ms of mixing the H200N–HPCA complex(es) with stoichiometric amounts of O_2, both doublets disappeared. The 20 ms spectrum is dominated by a new species (representing ~75% of the Fe) with a ΔE_Q of 0.95 mm/s and a δ of 0.48 mm/s. This species, called H200N$_{Int1}^{HPCA}$, has a δ value typical of high-spin Fe^{III} ($S_1 = {}^5/_2$). The observation of a quadrupole doublet at 4.2 K in zero field, rather than a spectrum exhibiting paramagnetic hyperfine structure, which is typical for isolated Fe^{III}, suggests that H200N$_{Int1}^{HPCA}$ has an overall zero or integer spin. This is consistent with the formulation of H200N$_{Int1}^{HPCA}$ that emerged from our EPR studies. Approximately 20–25% of the iron in the 20 ms sample belongs to an Fe^{II} species, perhaps multiple species, with a ΔE_Q of ≈3.10 mm/s and a δ of ≈1.20 mm/s (this species may give rise to the broad integer spin EPR spectrum of Figure 3B). As pointed out in Experimental Procedures, at high mixing speeds some of the material bounces off the aluminum wheel of the quencher and cools more slowly, leading to the appearance of later species in earlier time point samples. Our kinetic data indicate that the reaction has not progressed appreciably beyond H200N$_{Int1}^{HPCA}$ at 40 ms under the experimental conditions (Figure S2 of the Supporting Information), suggesting that the ferrous species in the 20 ms sample, which differ(s) from the substrate complexes, arises from this "splashed" material. A spectrum recorded for a sample quenched at 40 ms (not shown) was identical to the one obtained at 20 ms, showing that the amount of material attributed to splash is constant, as expected. At 400 ms, the fraction of iron in H200N$_{Int1}^{HPCA}$ has decreased to 50% of the Fe in the sample (Figure 4D). In this sample, approximately 10% of the Fe belongs to a doublet with a ΔE_Q of ≈2.30 mm/s and a δ of ≈1.10 mm/s (blue line in Figure 4D); this ferrous species is possibly another intermediate [tentative H200N$_{Int2}^{HPCA}$ (Table 2)]. Figure 4E shows a spectrum of a sample frozen (not by RFQ) at 180 s, a time where solution kinetics predict the product will have formed and dissociated (Figure S2 of the Supporting Information). However, the parameters of the observed doublet are as follows: $\Delta E_Q = 3.10$ mm/s, and $\delta = 1.20$ mm/s (>90% of Fe). They are slightly different from those of the substrate-free enzyme. It is possible that the high concentration of product present in the Mössbauer sample prevents net product dissociation or leads to a mixture of product-bound and free enzyme in this sample. Accordingly, this species is also present in the 400 ms sample (representing ~20% of Fe over and above the splashed material), a time at which approximately 25% of the enzyme is expected to be present in the product complex (Figure S2 of the Supporting

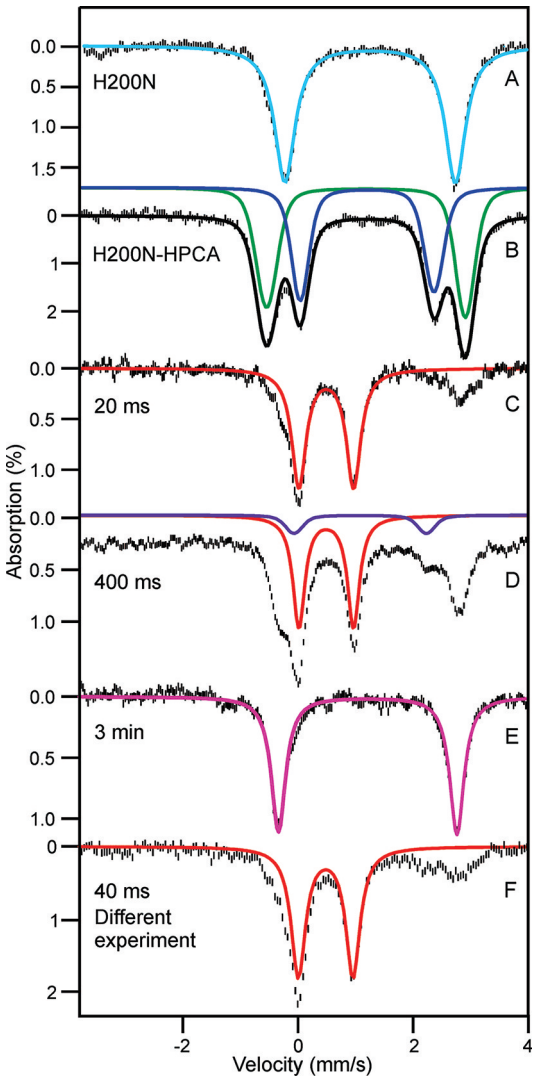

Figure 4. Zero-field Mössbauer spectra (4.2 K) of H200N−HPCA complexes. (A) H200N at 0.9 mM and pH 7.5 in 200 mM MOPS buffer. The colored line is a simulation. (B) Stoichiometric (sites) H200N−HPCA complex at 1.54 mM and pH 7.5 in 200 mM MOPS buffer. Simulations of the doublets of the two enzyme−substrate complexes, $H200N_{ES1}^{HPCA}$ (green) and $H200N_{ES2}^{HPCA}$ (blue), are depicted by the colored lines. The black line represents the sum of the two species. (C−E) Reaction of 1.48 mM H200N−HPCA with O_2-saturated buffer (1:1). For the RFQ samples quenched at (C) 20 and (D) 400 ms, we have outlined in red the spectrum of the intermediate, $H200N_{Int1}^{HPCA}$. (E) Sample frozen (not by RFQ) at 3 min representing the end of the reaction. The colored line is a simulation of the spectrum. (F) $B = 0$ spectrum of the RFQ sample of Figure 5 prepared in a different experiment under the same conditions.

Information). The product proved to be insufficiently stable to make an enzyme−product complex via addition of the purified product to the resting enzyme.

Figure 4F shows a zero-field spectrum from a different set of experiments for a sample quenched at 40 ms. The sample contains ∼70% of the Fe in $H200N_{Int1}^{HPCA}$ (red line). Figure 5 shows spectra of this sample taken in parallel applied fields of 4.0 and 8.0 T. The features observed are typical of high-spin Fe^{III} sites (the middle section of the spectra is contaminated by the unknown spectral features of the "splashed" ferrous species). We have analyzed the spectra of $H200N_{Int1}^{HPCA}$ with the spin Hamiltonian $H = H_e + H_{hf}$ (omitting the dipole−dipole term in H_e of eq 1), where H_{hf} describes the ^{57}Fe hyperfine interactions.

Table 2. Comparison of Quadrupole Splitting and Isomer Shift Parameters for the Mössbauer Spectra of FeHPCD and Its Variants and Complexes

species	ΔE_Q (mm/s)	δ (mm/s)	maximum percent present in the sample
FeHPCD	2.97(3)	1.23(2)	>90
H200N	3.01(3)	1.24(2)	>90
H200N−4NC[a]	3.57	1.12	>90
$FeHPCD_{ES1}^{HPCA}$	3.29(3)	1.14(2)	55
$FeHPCD_{ES2}^{HPCA}$	2.18(3)	1.18(2)	45
$H200N_{ES1}^{HPCA}$	3.45(3)	1.16(2)	60
$H200N_{ES2}^{HPCA}$	2.32(3)	1.20(2)	40
$FeHPCD_{Int1}^{HPCA}$	2.33(3)	1.08(2)	∼95[b]
$H200N_{Int1}^{HPCA}$	0.95(2)	0.48(1)	∼95[b]
$H200N_{Int2}^{HPCA}$	≈2.30	≈1.10	∼10

[a]From ref 19. [b]After correction for material splashed from the rapid freezing surface at high ram velocities.

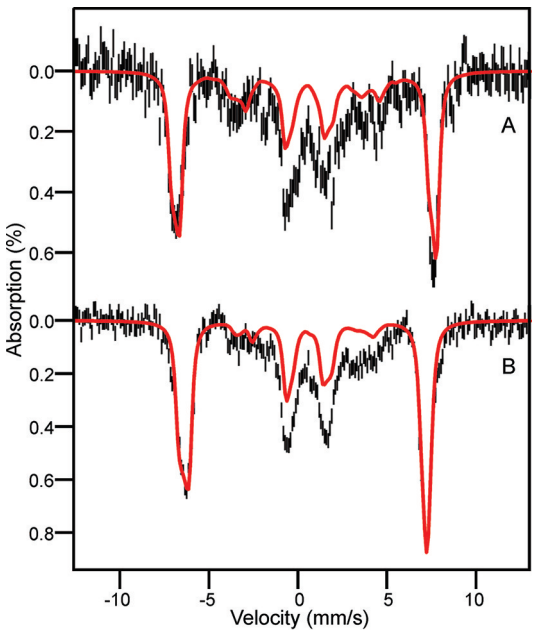

Figure 5. Mössbauer spectra (4.2 K) of $H200N_{Int1}^{HPCA}$ recorded in parallel applied magnetic fields of (A) 4.0 and (B) 8.0 T. The central features of the spectra have unresolved contributions from the splashed ferrous contaminant. The red lines, drawn to represent 70% of total Fe, are WMOSS spectral simulations based on eq 1 using the parameters listed in Table 1. The sample from Figure 4F was used.

$$\mathcal{H}_{hf} = A_0\mathbf{S}_1\cdot\mathbf{I}_1 + (eQV_{zz}/12)[3I_{1z}^2 - 15/4 + \eta(I_{1x}^2 - I_{1y}^2)] - g_n\beta_n B\cdot\mathbf{I}_1 \quad (3)$$

In eq 3, all symbols have their conventional meanings. For the ^{57}Fe magnetic hyperfine coupling constant of the ferric ion, we obtained $A_0/g_n\beta_n = -21.5 \pm 0.2$ T, which compares well with A_0 values reported for octahedral Fe^{III} sites with N/O coordination.[25] This observation, together with the observation that the δ value of $H200N_{Int1}^{HPCA}$ falls squarely into the center of high-spin ferric δ values, indicates that the iron is Fe^{III} with little delocalization between the radical and the ferric ion. From the field dependence of the Mössbauer spectra, we were able to

dx.doi.org/10.1021/bi201436n | Biochemistry 2011, 50, 10262−10274

constrain the zero-field splitting parameter, D_1, as follows. The observation of the $g = 8.2$ resonance implies that the EPR active doublet is split in zero field by $\Delta = (4/3)3D_1(E_1/D_1)^2 \approx 0.065$ cm^{-1} (4/3 is a spin projection factor that enters through consideration of exchange coupling when the EPR data are described by eq 2). The high-field Mössbauer spectra then constrain D_1 and $(E/D)_1$ to the reasonably narrow ranges of 1.1−1.4 cm^{-1} and 0.12−0.14, respectively. The red lines in Figure 5 are spectral simulations of $H200N_{Int1}^{HPCA}$ using the parameters listed in Table 1.

^{17}O Hyperfine Coupling Suggests That $H200N_{Int1}^{HPCA}$ Contains an Fe-Peroxo and a Substrate Radical Moiety. To further probe the nature of the $S_R = {}^1/_2$ species in $H200N_{Int1}^{HPCA}$, we have prepared samples enriched with ^{17}O in either $^{17}O_2$ or 3-^{17}OH-HPCA (^{17}O, $I^{17}_O = {}^5/_2$). Parallel mode EPR spectra of $H200N_{Int1}^{HPCA}$ prepared with $^{16}O_2$ (red), 70% enriched $^{17}O_2$ (blue), and 68% enriched 3-^{17}OH-HPCA (green) are shown in Figure 6. The $g = 8.2$ resonance of

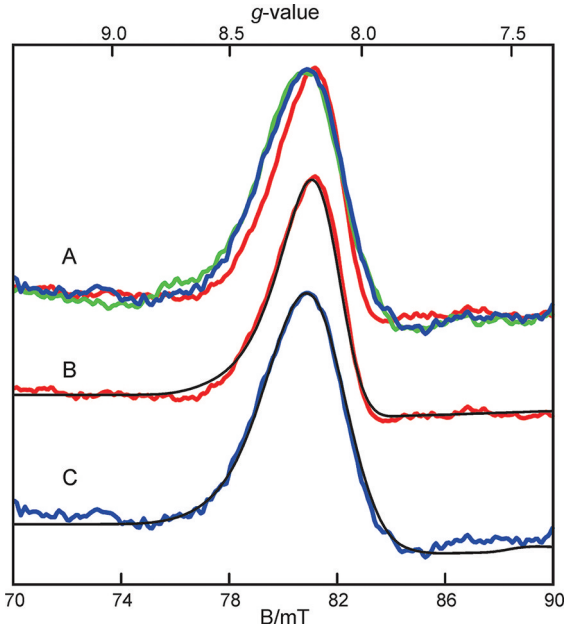

Figure 6. (A) EPR spectra of isotopically enriched $H200N_{Int1}^{HPCA}$ prepared with (red) natural abundance isotopes, (blue) 70% enriched $^{17}O_2$, and (green) HPCA enriched to 68% with ^{17}O at the C3 OH functional group. Samples were prepared as described in the legend of Figure 2. Conditions before mixing: 1.65 mM H200N−HPCA complex, saturated O_2-containing buffer, 200 mM MOPS (pH 7.5), and 4 °C. EPR conditions: frequency, 9.29 GHz; microwave power, 20 mW; modulation, 1 mT; temperature, 10 K. The simulations of natural abundance (B) and 70% enriched $^{17}O_2$ (C) samples are for $S = 2$, $D = 1.3$ cm^{-1}, and $E/D = 0.12$ with $A_z^{O,c}$ values of 0 (B) and 17 MHz (C).

both enriched samples is broadened relative to its ^{16}O counterpart. For the two samples, the broadening is the same within experimental uncertainty.

For our analysis of the ^{17}O broadenings, we used the $S = 2$ Hamiltonian of eq 2. As will be described shortly, the uncoupled representation of eq 1 is less suitable for this analysis. Using eq 2, SpinCount analysis yielded an $|A_z^{O,c}|$ of 17 MHz for both the $^{17}O_2$ and 3-^{17}OH-HPCA enriched samples. As mentioned above, the $^{17}O_2$ analysis assumes that only one ^{17}O nucleus contributes to the signal. The $g = 8.2$ resonance is observed when the applied field, B, is along the molecular z-direction defined by the zero-field splitting term of eq 2. Therefore, the spectra are sensitive to only A_z^O. We have considered whether the ^{17}O is part of the radical moiety (such as a superoxo radical) or whether it is part of a non-radical-bearing ligand coordinated to the iron. In the former case, the ^{17}O **A** tensor of the coupled representation is related to the intrinsic (uncoupled) hyperfine tensor by $\mathbf{A}^{O,c} = (-{}^1/_6)\mathbf{A}^O$, which yields an A_z^O of 102 MHz. In previous work, we have characterized a related intermediate species from the same mutant HPCD using 4NC as a substrate, identified as an Fe(III)−superoxo species.[19] The superoxo-based radical had a substantially larger A_z^O of 180 MHz, resulting in a profound broadening of the EPR signal, and different values of J, D_1, and $(E/D)_1$ (see Table 1). One might suspect that the reduced A_z^O reflects a superoxo radical that has donated significant negative spin density to the iron. However, if this were the case, we would have observed a larger Mössbauer isomer shift and the ^{57}Fe **A** tensor would exhibit substantial anisotropy because of a spin-dipolar term that would reflect the ferrous admixture to the site. This consideration is in marked contrast to what is observed here. We thus conclude that $H200N_{Int1}^{HPCA}$ does not contain a superoxo radical but instead contains a radical that resides on the HPCA moiety, presumably as an aromatic radical. Indeed, none of the other iron ligands are likely radical sites. The broadening from $^{17}O_2$ enrichment is therefore likely due to a peroxo species bound to the iron in a HPCA$^{\bullet}$−Fe^{III}−(hydro)peroxo complex. If the radical is located on the HPCA, the observed ^{17}O hyperfine coupling would be due to covalent spin polarization delocalization of the peroxo moiety by the ferric ion. In this case, the ^{17}O **A** tensor in the coupled representation is related to the intrinsic (uncoupled) hyperfine tensor by $\mathbf{A}^{O,c} = ({}^7/_6)\mathbf{A}^O$, from which we obtain an $|A_z^O|$ of 15 MHz.

The labeling of 3-^{17}OH-HPCA results in a broadening of the spectrum comparable to that of the $^{17}O_2$ sample. The interpretation of the broadening for 3-^{17}OH-HPCA is significantly more complex, because the C3 oxygen may have spin density contributions not only from coordination to the Fe^{III} but also from the HPCA radical. A covalent spin polarization contribution to the ^{17}O hyperfine interaction induced by the Fe^{III} has a favorable spin projection factor ($^7/_6$), compared to the factor of $-{}^1/_6$ for the case in which the radical resides on the HPCA moiety (note that the use of eq 1, rather than eq 2, would bias the primary analysis of the EPR spectra). Thus, for comparable spin density contributions to the labeled O (Fe vs HPCA$^{\bullet}$) the A value would be dominated by the contribution from the Fe^{III}. In the absence of quantitative insight about the source of the spin density at the C_3 oxygen by quantum chemical calculations, it seems prudent to reserve judgment about the precise origin of the broadening by 3-^{17}OH-HPCA.[b]

Stopped-Flow Spectroscopy of the FeHPCA + O_2 Reaction Reveals No Evidence of an Intermediate Similar to $H200N_{Int1}^{HPCA}$. Figure 7 shows diode spectra from the single-turnover reaction in which a preformed, anaerobic, stoichiometric FeHPCD−HPCA substrate complex is rapidly mixed with O_2-containing buffer at 4 °C. The spectra show only formation of the ring-cleaved product with a λ_{max} near 380 nm with no detectable chromophore in the lower-energy region from 500 to 700 nm; reaction of a 1 mM FeHPCD−HPCA sample also failed to show a long wavelength band. However, kinetic analysis of product formation using a single-wavelength trace at 380 nm has previously revealed that product formation

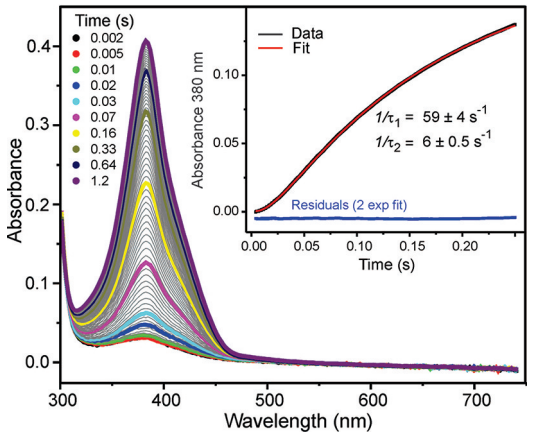

Figure 7. FeHPCD−HPCA + O_2 reaction monitored by the stopped-flow method. Diode array spectra recorded from 4 ms to 2 s after mixing 100 μM (based on active sites) stoichiometric, anaerobic FeHPCD−HPCA complex with O_2-saturated buffer (~1.8 mM) at 4 °C in 200 mM MOPS (pH 7.5) (2 mm path length). The inset shows the reaction monitored by single-wave stopped-flow spectroscopy at 380 nm. In the time range shown, the data (black line) can be fit to a sum of two exponential terms (red line) with the reciprocal relaxation times shown.

proceeds in several phases, including a fast phase that decays with a k_1 of ~38 s^{-1} and a slower phase with a k_2 of ~3.8 s^{-1}.[20]

In the preparations described here, both rates are slightly faster (k_1 = 59 ± 4 s^{-1}, and k_2 = 6.0 ± 0.5 s^{-1}). The fast phase is associated with a lag in product formation as shown in the inset of Figure 7 and precedes formation of the product chromophore. Consequently, while there are discrete intermediates in the oxygen activation and insertion processes, none of the detectable intermediates have optical features like those of H200N$_{Int1}^{HPCA}$. After the FeHPCD−HPCA complex had been mixed with O_2, single-wavelength data at 380 nm (Figure 7, inset) show that the lag phase persists to ~30 ms, providing an opportunity to use the RFQ approach for trapping reaction intermediates that precede product formation in the FeHPCD + O_2 reaction.

RFQ Samples from the FeHPCD + O_2 Reaction Reveal an Fe^{II} Reaction Intermediate. Because both the H200N−4NC + O_2 and H200N−HPCA + O_2 reactions have revealed high yields of oxygenated intermediates at times of <1 s (Figures 1−6[19]), we have prepared RFQ samples from the wild-type (WT) FeHPCD−HPCA + O_2 reaction to look for reaction intermediates associated with the lag phase in the kinetic time course before product formation.

The Mössbauer spectrum of the resting state WT enzyme consists of one doublet with a ΔE_Q of 2.97 mm/s and a δ of 1.23 mm/s, consistent with a six-coordinate high-spin Fe^{II} species (Figure 8A).[2,23] Anaerobic addition of HPCA to the resting state WT enzyme yields a Mössbauer spectrum consisting of two ferrous doublets (Figure 8B). One doublet accounts for 55% of the iron with a ΔE_Q of 3.29 mm/s and a δ of 1.14 mm/s [FeHPCD$_{ES1}^{HPCA}$ (Table 2)], while the other species has 45% of the iron giving a doublet with a ΔE_Q of 2.18 mm/s and a δ of 1.18 mm/s [FeHPCD$_{ES2}^{HPCA}$ (Table 2)].[a] Note that these parameters differ from those observed for the H200N−HPCA complex. The spectrum of a sample frozen at 15 ms, which is within the lag phase of the FeHPCD−HPCA + O_2 reaction, is shown in Figure 8C. It reveals two new species exhibiting quadrupole doublets from ferrous ions. One doublet

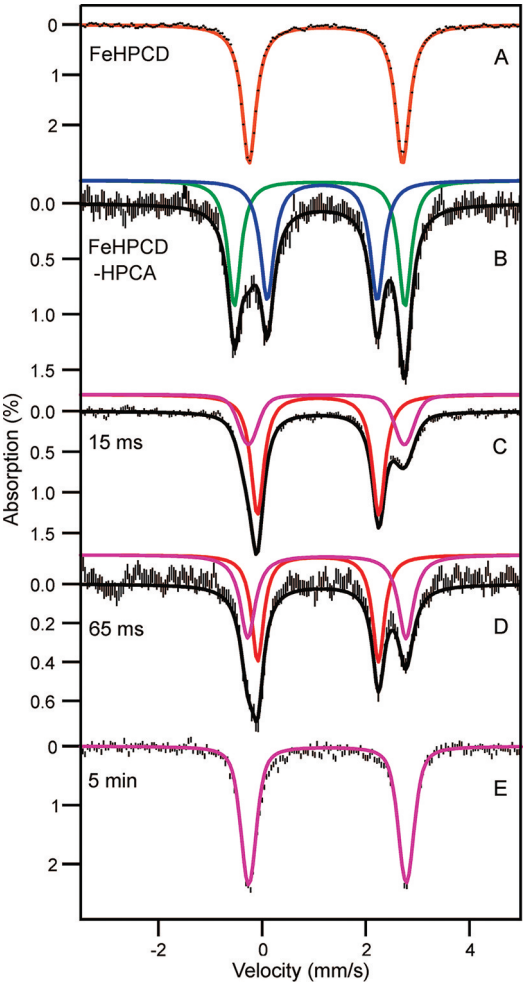

Figure 8. Mössbauer spectra from the FeHPCD−HPCA + O_2 reaction recorded at 4.2 K for B = 0: (A) FeHPCD, (B) anaerobic FeHPCD−HPCA complex, (C) FeHPCD−HPCA and O_2 15 ms after the sample had been mixed with O_2, (D) FeHPCD−HPCA and O_2 65 ms after the sample had been mixed with O_2, and (E) FeHPCD−HPCA and O_2 5 min after the sample had been mixed with O_2. Conditions before mixing: ~1.8 mM enzyme−substrate complex, 200 mM MOPS, pH 7.5, and 4 °C for all reactions. For spectrum A, the sample concentration was ~0.9 mM.

has a ΔE_Q of 2.33 mm/s and a δ of 1.08 mm/s [FeHPCD$_{Int1}^{HPCA}$ (Table 2)] and accounts for ~70% of the iron. This species appears to decay to the second species that has parameters similar to those of the resting state enzyme (ΔE_Q = 3.03 mm/s, and δ = 1.24 mm/s) (Figure 8D). This second species amounts to ~95% of the signal shown at the end of the reaction (Figure 8E). It is not clear whether this is the product-free resting enzyme or enzyme with product still bound because of its relatively high concentration in the Mössbauer sample. Its presence in the 15 ms sample may again be due to splash from the freezing wheels at high ram velocity. Our combined stopped-flow and RFQ/Mössbauer data suggest that FeHPCD$_{Int1}^{HPCA}$ is a ferrous reaction intermediate that accumulates to nearly quantitative yields in the reaction cycle of the WT enzyme.

DISCUSSION

The isolation and characterization of the intermediates that follow binding of O_2 in the reaction cycle of Fe^{II}-containing

dx.doi.org/10.1021/bi201436n | Biochemistry 2011, 50, 10262−10274

catechol dioxygenases such as FeHPCD have been elusive goals. Our recent characterization of the relatively long-lived intermediates in the reaction of H200N−4NC with O_2 was informative; however, the reaction leads to ring oxidation rather than ring cleavage.[18,19] The short lifetimes of intermediates in the reaction cycles of WT and mutant enzymes catalyzing ring cleavage reactions present a greater challenge. Here, the intermediates formed after oxygen binding in the H200N- and FeHPCD-catalyzed ring cleavage of HPCA have been trapped for spectroscopic characterization and comparison. The results show that the first intermediates trapped after addition of O_2 in each of these systems differ fundamentally from each other as well as from the 4NC−Fe^{III}−superoxo intermediate trapped in the non-ring-cleaving H200N−4NC + O_2 system. The structural insights gained from the evaluation of the spectra of these intermediates and the relevance to the mechanism of O_2 activation for aromatic ring cleavage are discussed here.

Identity of $H200N_{Int1}^{HPCA}$. The studies described here show that $H200N_{Int1}^{HPCA}$ contains a high-spin Fe^{III} ($S_1 = {}^5/_2$) site that is antiferromagnetically coupled to a radical ($S_R = {}^1/_2$) to yield an $S = 2$ ground multiplet. The ^{57}Fe magnetic hyperfine coupling of $H200N_{Int1}^{HPCA}$ ($A_0/g_n\beta_n = -21.5$ T) compares well to those observed for mononuclear Fe^{III} sites, and the isomer shift (δ = 0.48 mm/s) is characteristic of octahedral high-spin Fe^{III} sites with N/O ligands (Table 1).[2,19,23,26] As judged by the values of A_0 and δ, one electron has been transferred from the Fe^{II}. A radical species that couples to the resulting Fe^{III} must have been formed either directly or indirectly as a result of this transfer.

The most likely candidates for the $S_R = {}^1/_2$ species bound to the Fe^{III} are suggested by the two intermediates discovered during our previous study of the H200N−4NC + O_2 reaction, namely, $H200N_{Int1}^{4NC}$ formulated as 4NC−Fe^{III}−$O_2^{\bullet-}$ and $H200N_{Int2}^{4NC}$ formulated as 4NC$^{\bullet}$−Fe^{III}−(hydro)peroxo. The spectroscopic data for $H200N_{Int1}^{HPCA}$ are overall quite similar to those of the latter, $H200N_{Int2}^{4NC}$, and differ significantly from those of the former. Specific similarities include Mössbauer parameters, EPR spectra, substantial positive J values (antiferromagnetic), a positive D_1 value, and small ^{17}O hyperfine constants. In contrast, the 4NC−Fe^{III}−$O_2^{\bullet-}$ complex has a much smaller J value (6 cm^{-1}) and a negative D_1 value, and its EPR signal is significantly more broadened when $^{17}O_2$ is used. Thus, we propose that $H200N_{Int1}^{HPCA}$ is formulated as HPCA$^{\bullet}$−Fe^{III}−(hydro)peroxo.[b]

The HPCA-SQ$^{\bullet}$ as the site of the radical is in accord with the crystallographic structure of the oxy intermediate formed in the reaction of FeHPCD−4NC with O_2, which revealed substantial ring deformation at the carbon where oxygen subsequently attacks to form the alkylperoxo intermediate. This suggests that a localized radical forms at this carbon of the ring.[12] However, the 2.4 Å bond lengths from the metal ligands to the bound dioxygen species that we see in this intermediate suggest that the iron is in the Fe^{II} state. This would mean that the bound oxygen is likely to be superoxo rather than peroxo.

The UV−vis spectrum of $H200N_{Int1}^{HPCA}$ shows three main features, namely, a high-energy shoulder at ∼310 nm ($\varepsilon_{310} \sim$ 7000 M^{-1} cm^{-1}), a maximum at 395 nm ($\varepsilon_{395} \sim$ 3200 M^{-1} cm^{-1}), and a lower-energy feature near 610 nm ($\varepsilon_{610} \sim$ 1100 M^{-1} cm^{-1}). This spectrum is inconsistent with HPCA bound in the catecholic form.[27−29] The two higher-energy features are similar to those observed for unbound catechol quinones and semiquinones, which themselves have similar spectra (Table S2 of the Supporting Information).[30,31] Indeed, the spectrum of $H200N_{Int1}^{HPCA}$ in the 300−500 nm region is very similar to that of HPCA quinone (Figure 1A, inset, blue dashed spectrum). Binding of these molecules to oxidized metals causes little change in the band positions or intensities. However, the semiquinone complexes can give rise to additional charge transfer bands in the 600−800 nm region with widely ranging extinction coefficients (300−3000 M^{-1} cm^{-1}) (Table S2 of the Supporting Information).[32,33] Very few $S = 2$ ligand−Fe^{III}−SQ$^{\bullet}$ model complexes have been spectroscopically characterized, but those available show similar optical characteristics (Table S2 of the Supporting Information).[33−35] When considered in light of the EPR and Mössbauer analysis, the optical spectrum of $H200N_{Int1}^{HPCA}$ is most consistent with a HPCA-SQ$^{\bullet}$ radical and peroxo ligands bound to Fe^{III}.

While the 610 nm chromophore may derive from an HPCA-SQ$^{\bullet}$−Fe^{III} interaction, another possibility is a (hydro)peroxo-to-Fe^{III} LMCT band, given the structure of $H200N_{Int1}^{HPCA}$ proposed here. A band in this region might also arise from an Fe^{III}−OOR complex, but in the current case, this would be the alkylperoxo intermediate of the reaction cycle that is expected to contain Fe^{II} based on computational studies.[36,37] Many end-on Fe^{III}−OOH and side-on bound Fe^{III}−O_2^{2-} complexes from non-heme mononuclear model complexes have been characterized (Table S2 of the Supporting Information).[38,39] The Fe^{III}−OOH complexes are often low-spin when the iron is coordinated by nitrogen ligands, but incorporation of at least one carboxylate ligand can result in a high-spin Fe^{III}−OOH complex as would pertain to the intermediates of FeHPCD. In comparison to the 610 nm species observed here, the high-spin Fe^{III}−OOH model complexes generally have a UV−vis transition with comparable intensity (ε = 450−2000 M^{-1} cm^{-1}) but a shorter λ_{max} (440−570 nm) (Table S2 of the Supporting Information).[38,39]

In model compounds, it has been shown that the Fe^{III}−OOH complexes can be deprotonated to form the conjugate base side-on bound Fe^{III}−O_2^{2-} complex at pH >10.[38,39] In such a case, the resultant complex is often high-spin, exhibiting a λ_{max} shift into the range of the 610 nm species ($\lambda_{max} \sim$ 525−750 nm), but the ε values (450−600 M^{-1} cm^{-1}) are lower. Many of these side-on peroxo species have an EPR spectrum originating from an excited state like $H200N_{Int1}^{HPCA}$, but the Mössbauer isomer shift is somewhat larger (0.66 mm/s vs 0.48 mm/s). A third possibility is suggested by the high-spin Fe^{III}−(hydro)-peroxo intermediate in benzoate 1,2-dioxygenase, which we know from the crystal structure of the equivalent intermediate found in naphthalene 1,2-dioxygenase to be a side-on bound Fe^{III} species.[40] Our spectroscopic analysis of the species from benzoate 1,2-dioxygenase shows that the Mössbauer isomer shift is 0.5 mm/s, as found for $H200N_{Int1}^{HPCA}$. We have proposed that this is due to protonation of the side-on bound peroxo moiety.[41] If this is the case, a pH dependence might be expected for the low-energy band of the $H200N_{Int1}^{HPCA}$ spectrum, but none is observed in the range between pH 5.5 and 9.0 (Figure 1B, inset). One possible explanation for this is that the pK_a for this type of species is relatively high, as observed for the end-on hydroperoxo complexes, such that it remains protonated throughout the range of stability for the enzyme. On the basis of this analysis, it is not currently possible to definitively assign the origin of the 610 nm species, and it could, in fact, result from the sum of both Fe^{III}−HPCA-SQ$^{\bullet}$ and Fe^{III}−(hydro)peroxo interactions.

Identity of $H200N_{Int2}^{HPCA}$. Analysis of transient kinetic data from the time course of the 610 nm intermediate as well as product formation in the H200N−HPCA + O_2 reaction (values

from the current preparation are shown in Figures S1 and S2 of the Supporting Information and Scheme 2)[18] suggests that

Scheme 2. Kinetic Model from Stopped-Flow Studies of the H200N−HPCA + O_2 Reaction

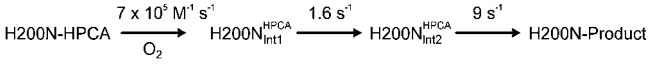

$H200N_{Int1}^{HPCA}$ accumulates to near stoichiometric yield. This is in accord with the Mössbauer and EPR spectra of this reaction intermediate shown here. On the other hand, the kinetic model predicts $H200N_{Int2}^{HPCA}$ would accumulate to a level of only ~12% at 400 ms because of the rapid decay of the species (Figure S2 of the Supporting Information). Analysis of the Mössbauer reaction time course does show that $H200N_{Int2}^{HPCA}$ accumulates to a level of only ~10% at 400 ms (Figure 6C). Because of low yields of $H200N_{Int2}^{HPCA}$, we were unable to obtain the precise Mössbauer parameters of this species. However, it is clear that $H200N_{Int2}^{HPCA}$ is ferrous with a ΔE_Q of ≈2.33 mm/s and a δ of ≈1.1−1.2 mm/s. It is possible that this species is either the predicted (Scheme 1D) $HPCA^{\bullet}-Fe^{II}-O_2^{\bullet-}$ complex or, perhaps more likely, the Fe^{II}−alkylperoxo or lactone intermediates, which derive from $H200N_{Int1}^{HPCA}$ prior to formation of the yellow ring-cleaved product.

Identity of $FeHPCD_{Int1}^{HPCA}$. The Mössbauer parameters for $FeHPCD_{Int1}^{HPCA}$ show that this reaction intermediate contains a high-spin Fe^{II} site, in sharp contrast to the Fe^{III}-containing initial intermediates described here and in our earlier study.[19] Unlike the case for $H200N_{Int1}^{HPCA}$, no optical spectrum of this intermediate could be detected even in the first few milliseconds of the reaction. Consequently, our stopped-flow studies of the FeHPCD−HPCA + O_2 reaction were limited to monitoring product formation, which is clearly a process with at least two steps.[20] The largest reciprocal relaxation time from this process makes the largest contribution to the observed lag phase and shows no O_2 concentration dependence. Thus, it is dominated by the rate constants for a step separated from the initial O_2 binding by at least one irreversible step. $FeHPCD_{Int1}^{HPCA}$ is temporally associated with this initial lag in product formation, suggesting that it occurs after the effectively irreversible step in the reaction. The lack of an optical spectrum from a semiquinone or quinone for $FeHPCD_{Int1}^{HPCA}$ is consistent with this hypothesis and also argues against a HPCA-$SQ^{\bullet}$−$Fe^{II}-O_2^{\bullet-}$ or HPCA quinone−Fe^{II}−(hydro)peroxo structure. $FeHPCD_{Int1}^{HPCA}$ cannot be a product complex that would be intensely yellow even before dissociation from the enzyme; the true product complex builds on a much longer time scale. Taken together, these observations suggest $FeHPCD_{Int1}^{HPCA}$ is one of the intermediates that results after oxygen attacks the substrate, but before ring cleavage, such as the alkylperoxo or lactone intermediates of the proposed reaction cycle. Accordingly, the Mössbauer parameters for this species are very similar to those of $H200N_{Int2}^{HPCA}$, which is postulated above to be such a species.

Mechanistic Implications of the Observed Intermediates. Our studies of the intermediates of the O_2 activation and insertion portion of the extradiol dioxygenase reaction cycle have shown that the nature and reactivity of the intermediates are functions of both the electronic characteristics of the substrate and the amino acid residues present in the second sphere of the active site. Scheme 3 illustrates the intermediates that have been trapped and characterized by various means.

Scheme 3. Intermediates from the FeHPCD and H200N Turnover Cycles[a]

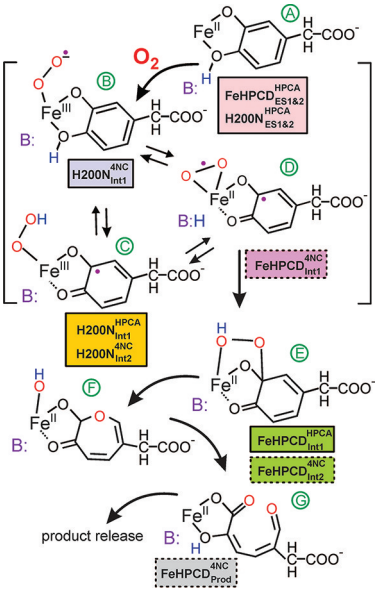

[a]The intermediates shown are those proposed for the reaction of FeHPCD with HPCA as the substrate. The colored boxes identify trapped intermediates that either correlate exactly with or are similar to these intermediates. The boxes with solid borders identify intermediates from solution RFQ studies reported here and in a previous study,[19] while those with dashed borders are from crystal structures reported previously.[12]

Studies thus far have focused on substrates with progressively more electron withdrawing para substituents and mutation of the key acid/base catalyst, His200. It is found that when a shorter Asn residue is substituted for His200, two types of intermediates can rapidly form in nearly 100% yield, both of which contain Fe^{III} spin-coupled to a radical. More specifically, an end-on bound $Fe^{III}-O_2^{\bullet-}$ adduct is formed when the substrate has a strongly electron-withdrawing *p*-nitro substituent (Scheme 3B),[19] whereas a substrate $SQ^{\bullet}-Fe^{III}$−(hydro)peroxo species (peroxo orientation is not definitively determined) is formed when HPCA with its electron-donating substituent is used (Scheme 3C). These two intermediates differ substantially not only in their respective lifetimes but also in the eventual outcomes of catalysis.

The $4NC-Fe^{III}-O_2^{\bullet-}$ intermediate persists for many minutes and eventually yields 4NC-quinone and H_2O_2, whereas the HPCA-$SQ^{\bullet}-Fe^{III}$−(hydro)peroxo intermediate disappears in 2 s at 4 °C and yields the normal ring-cleaved product. The ability of O_2 to bind to the enzyme is also affected by the para substituent of the substrate in the H200N mutant such that the binding rate constant is 4-fold slower and the reaction becomes reversible when 4NC is bound in place of HPCA.[18] These observations suggest that the effects of either electron withdrawal or donation in the substrate ring are transmitted through the iron to affect its ability to share electrons with the O_2 during binding. We have proposed that this transmission of electron density from the substrate through the iron to the bound O_2 is a fundamental aspect of oxygen activation in this enzyme family.[10,12,13]

The reaction of the native enzyme with 4NC and HPCA reveals other aspects of the mechanism. When His200 is present, substrates with electron-withdrawing or -donating

substituents are converted into ring-cleaved products, albeit at 25-fold different rates. The crystallographically characterized intermediate in the reaction of FeHPCD−4NC with O_2 ($FeHPCD^{4NC}_{Int1}$) (Scheme 3D)[12] and the spectroscopically characterized $FeHPCD^{HPCA}_{Int1}$ intermediate (Scheme 3E) described here both have Fe^{II} in the active site rather than Fe^{III}. However, the former appears to be a species with radical character on both the substrate and the bound O_2, while it is argued above that the latter is likely to be a state after the attack of oxygen on the substrate. If this is the case, then the formation and reaction of the reactive oxygen intermediate(s) must be very fast such that there is no evidence of any of the types of spin-coupled Fe^{III} intermediates described here or in our previous study. This may mean that an Fe^{III} species of some sort forms, but its lifetime is too short to be detected even on the millisecond time scale. Alternatively, the iron may serve purely as a conduit for electron density that does not change oxidation state as an electron is transferred from the catechol to O_2. The final alternative, namely, that there is no transfer of electron density between the substrates, is unlikely because the reaction of unactivated oxygen with catechols is slow and does not result in ring cleavage.

CONCLUSION

The oxy intermediates that have been trapped thus far using FeHPCD and its variants with HPCA and alternative substrates show that a radical species can reside on either the substrate or the oxygen and that an electron can be transferred from the iron, the substrate, or both to the oxygen. On the basis of the *in crystallo* studies published previously,[12] it is possible for an electron to be transferred in either a stepwise or a concerted fashion from the iron to the oxygen and from the substrate to the iron to yield a diradical pair. All of these observations support the most fundamental aspect of catalysis established for this enzyme class, which envisions oxygen activation by coordinating oxygen reduction with substrate oxidation to form a reactive pair. The results reported in our previous study show that simple formation of an $Fe^{III}-O_2^{\bullet-}$ species alone is not sufficient for high reactivity or ring cleaving chemistry. This study suggests that, following the transfer of an electron from the substrate, either a substrate $SQ^{\bullet}-Fe^{II}-O_2^{\bullet-}$ or a substrate $SQ^{\bullet}-Fe^{III}$−peroxo intermediate might serve as the reactive species. However, the high reactivity of the enzyme containing Fe^{II}, Mn^{II}, or Co^{II} [15,16] favors the substrate $SQ^{\bullet}-Fe^{II}-O_2^{\bullet-}$ species, for which there is no net change in oxidation state between the enzyme−substrate complex and the reactive species. Although this study suggests for the first time that a substrate $SQ^{\bullet}-Fe^{III}$−peroxo intermediate can lead to ring cleavage, its low rate of reaction suggests that it is not the species that conducts this reaction in the reaction cycle of the WT enzyme. It is notable that the maximal rate of O_2 activation and reaction is achieved only when His200 is present. This is consistent with our previous proposal that this residue plays many roles over and above its role as an acid/base catalyst.[18] These may include charge stabilization that promotes formation of the $SQ^{\bullet}-Fe^{II}-O_2^{\bullet-}$ species as well as hydrogen bonding and steric interactions that properly orient the superoxo species for reaction with the activated substrate.

ASSOCIATED CONTENT

Supporting Information

Methods for mass spectroscopic analysis of 3-^{17}OH-HPCA, Tables S1 and S2, and Figures S1 and S2. This material is available free of charge via the Internet at http://pubs.acs.org.

AUTHOR INFORMATION

Corresponding Author

*M.P.H.: Department of Chemistry, Carnegie Mellon University, 4400 Fifth Ave., Pittsburgh, PA 15213; e-mail, Hendrich@andrew.cmu.edu; phone, (412) 268-1058; fax, (412) 268-1061. E.M.: Department of Chemistry, Carnegie Mellon University, 4400 Fifth Ave., Pittsburgh, PA 15213; e-mail, EMunck@cmu.edu; phone, (412) 268-5058. J.D.L.: Department of Biochemistry, Molecular Biology, and Biophysics, 6-155 Jackson Hall, University of Minnesota, 321 Church St. SE, Minneapolis, MN 55455; phone, (612) 625-6454; fax, (612) 624-5121; e-mail, Lipsc001@umn.edu.

Funding

This work is supported by National Institutes of Health Grants GM 24689 (to J.D.L.), EB-001475 (to E.M.), and GM77387 (to M.P.H.) and Graduate Traineeship GM08700 (to M.M.M.).

ACKNOWLEDGMENTS

We thank Dr. David P. Ballou for the generous gift of the C1 and C2 enzymes used for synthesis of ^{17}O-labeled HPCA.

ABBREVIATIONS

FeHPCD, recombinant homoprotocatechuate 2,3-dioxygenase from *B. fuscum*; MnHPCD, recombinant homoprotocatechuate 2,3-dioxygenase from *B. fuscum* in which the Fe^{II} is replaced with Mn^{II}; H200N, His200Asn variant of FeHPCD; HPCA, homoprotocatechuate or 3,4-dihydroxyphenylacetate; 4NC, 4-nitrocatechol; WT, wild type; RFQ, rapid-freeze-quench; $SQ^{\bullet}$, semiquinone radical; $H200N^{4NC}_{Int1}$, spin-coupled high-spin 4NC−Fe^{III}−superoxo complex of H200N; $H200N^{4NC}_{Int2}$, spin-coupled high-spin 4NC-$SQ^{\bullet}$−Fe^{III}−(hydro)peroxo complex of H200N; $H200N^{HPCA}_{Int1}$ and $H200N^{HPCA}_{Int2}$, intermediates observed in the H200N−HPCA + O_2 reaction; $FeHPCD^{HPCA}_{Int1}$, intermediate observed in the FeHPCD−HPCA + O_2 reaction; $H200N^{HPCA}_{ES1}$, $H200N^{HPCA}_{ES2}$, $FeHPCD^{HPCA}_{ES1}$, and $FeHPCD^{HPCA}_{ES2}$, substrate complexes of H200N or FeHPCD with the substrate HPCA; EPR, electron paramagnetic resonance; LMCT, ligand to metal charge transfer transition.

ADDITIONAL NOTES

[a]The origin of the two enzyme−substrate species remains unknown. Crystal structures of enzyme−substrate complexes show that the small molecule ligand site of the iron has variable solvent occupancy, offering a possible source of heterogeneity. [b]Very little EPR line width change was observed when uniformly enriched [^{13}C]HPCA was used (data not shown). Because the ^{13}C would be part of the radical moiety, the spin projection factor ($-^1/_6$) would strongly suppress the broadening. Ongoing DFT computations showed that the ^{13}C enrichment would not broaden the g = 8.2 resonance to any significant extent even if the radical would be centered on labeled carbon.

REFERENCES

(1) Lipscomb, J. D., and Orville, A. M. (1992) Mechanistic aspects of dihydroxybenzoate dioxygenases. *Metal Ions Biol. Syst. 28*, 243−298.

(2) Arciero, D. M., Lipscomb, J. D., Huynh, B. H., Kent, T. A., and Münck, E. (1983) EPR and Mössbauer studies of protocatechuate 4,5-dioxygenase. Characterization of a new Fe^{2+} environment. *J. Biol. Chem. 258*, 14981−14991.

(3) Boldt, Y. R., Sadowsky, M. J., Ellis, L. B. M., Que, L., and Wackett, L. P. (1995) A manganese-dependent dioxygenase From *Arthrobacter globiformis* CM-2 belongs to the major extradiol dioxygenase family. *J. Bacteriol. 177*, 1225−1232.

(4) Vaillancourt, F. H., Bolin, J. T., and Eltis, L. D. (2006) The ins and outs of ring-cleaving dioxygenases. *Crit. Rev. Biochem. Mol. Biol. 41*, 241−267.

(5) Kovaleva, E. G., Neibergall, M. B., Chakrabarty, S., and Lipscomb, J. D. (2007) Finding intermediates in the O_2 activation pathways of non-heme iron oxygenases. *Acc. Chem. Res. 40*, 475−483.

(6) Dagley, S. (1978) Microbial catabolism, the carbon cycle and environmental pollution. *Naturwissenschaften 65*, 85−95.

(7) Bugg, T. D. H., and Winfield, C. J. (1998) Enzymic cleavage of aromatic rings: Mechanistic aspects of the catechol dioxygenases and later enzymes of bacterial oxidative cleavage pathways. *Nat. Prod. Rep. 15*, 513−530.

(8) Hegg, E. L., and Que, L. (1997) The 2-His-1-carboxylate facial triad: An emerging structural motif in mononuclear non-heme iron(II) enzymes. *Eur. J. Biochem. 250*, 625−629.

(9) Arciero, D. M., Orville, A. M., and Lipscomb, J. D. (1985) [^{17}O]Water and nitric oxide binding by protocatechuate 4,5-dioxygenase and catechol 2,3-dioxygenase. Evidence for binding of exogenous ligands to the active site Fe^{2+} of extradiol dioxygenases. *J. Biol. Chem. 260*, 14035−14044.

(10) Arciero, D. M., and Lipscomb, J. D. (1986) Binding of ^{17}O-labeled substrate and inhibitors to protocatechuate 4,5-dioxygenase-nitrosyl complex. Evidence for direct substrate binding to the active site Fe^{2+} of extradiol dioxygenases. *J. Biol. Chem. 261*, 2170−2178.

(11) Kovaleva, E. G., and Lipscomb, J. D. (2008) Versatility of biological non-heme Fe(II) centers in oxygen activation reactions. *Nat. Chem. Biol. 4*, 186−193.

(12) Kovaleva, E. G., and Lipscomb, J. D. (2007) Crystal structures of Fe^{2+} dioxygenase superoxo, alkylperoxo, and bound product intermediates. *Science 316*, 453−457.

(13) Shu, L., Chiou, Y. M., Orville, A. M., Miller, M. A., Lipscomb, J. D., and Que, L. Jr. (1995) X-ray absorption spectroscopic studies of the Fe(II) active site of catechol 2,3-dioxygenase. Implications for the extradiol cleavage mechanism. *Biochemistry 34*, 6649−6659.

(14) Spence, E. L., Langley, G. J., and Bugg, T. D. H. (1996) Cis-trans isomerization of a cyclopropyl radical trap catalyzed by extradiol catechol dioxygenases: Evidence for a semiquinone intermediate. *J. Am. Chem. Soc. 118*, 8336−8343.

(15) Emerson, J. P., Kovaleva, E. G., Farquhar, E. R., Lipscomb, J. D., and Que, L. Jr. (2008) Swapping metals in Fe- and Mn-dependent dioxygenases: Evidence for oxygen activation without a change in metal redox state. *Proc. Natl. Acad. Sci. U.S.A. 105*, 7347−7352.

(16) Fielding, A. J., Kovaleva, E. G., Farquhar, E. R., Lipscomb, J. D., and Que, L. Jr. (2011) A hyperactive cobalt-substituted extradiol-cleaving catechol dioxygenase. *J. Biol. Inorg. Chem. 16*, 341−355.

(17) Gunderson, W. A., Zatsman, A. I., Emerson, J. P., Farquhar, E. R., Que, L., Lipscomb, J. D., and Hendrich, M. P. (2008) Electron paramagnetic resonance detection of intermediates in the enzymatic cycle of an extradiol dioxygenase. *J. Am. Chem. Soc. 130*, 14465−14467.

(18) Groce, S. L., and Lipscomb, J. D. (2005) Aromatic ring cleavage by homoprotocatechuate 2,3-dioxygenase: Role of His200 in the kinetics of interconversion of reaction cycle intermediates. *Biochemistry 44*, 7175−7188.

(19) Mbughuni, M. M., Chakrabarti, M., Hayden, J. A., Bominaar, E. L., Hendrich, M. P., Münck, E., and Lipscomb, J. D. (2010) Trapping and spectroscopic characterization of an Fe^{III}-superoxo intermediate from a nonheme mononuclear iron-containing enzyme. *Proc. Natl. Acad. Sci. U.S.A. 107*, 16788−16793.

(20) Groce, S. L., Miller-Rodeberg, M. A., and Lipscomb, J. D. (2004) Single-turnover kinetics of homoprotocatechuate 2,3-dioxygenase. *Biochemistry 43*, 15141−15153.

(21) Jollie, D. R., and Lipscomb, J. D. (1990) Formate dehydrogenase from *Methylosinus trichosporium* OB3b. *Methods Enzymol. 188*, 331−334.

(22) Miller, M. A., and Lipscomb, J. D. (1996) Homoprotocatechuate 2,3-dioxygenase from *Brevibacterium fuscum*: A dioxygenase with catalase activity. *J. Biol. Chem. 271*, 5524−5535.

(23) Münck, E. (2000) Aspects of ^{57}Fe Mössbauer spectroscopy. In *Physical Methods in Bioinorganic Chemistry* (Que, L., Jr., Ed.) pp 287−319, University Science Books, Sausalito, CA.

(24) Sucharitakul, J., Chaiyen, P., Entsch, B., and Ballou, D. P. (2005) The reductase of p-hydroxyphenylacetate 3-hydroxylase from *Acinetobacter baumannii* requires p-hydroxyphenylacetate for effective catalysis. *Biochemistry 44*, 10434−10442.

(25) Whittaker, J. W., Lipscomb, J. D., Kent, T. A., and Münck, E. (1984) *Brevibacterium fuscum* protocatechuate 3,4-dioxygenase. Purification, crystallization, and characterization. *J. Biol. Chem. 259*, 4466−4475.

(26) Wolgel, S. A., Dege, J. E., Perkins-Olson, P. E., Jaurez-Garcia, C. H., Crawford, R. L., Münck, E., and Lipscomb, J. D. (1993) Purification and characterization of protocatechuate 2,3-dioxygenase from *Bacillus macerans*: A new extradiol catecholic dioxygenase. *J. Bacteriol. 175*, 4414−4426.

(27) Costas, M., Mehn, M. P., Jensen, M. P., and Que, L. Jr. (2004) Dioxygen activation at mononuclear nonheme iron active sites: Enzymes, models, and intermediates. *Chem. Rev. 104*, 939−986.

(28) Cox, D. D., Benkovic, S. J., Bloom, L. M., Bradley, F. C., Nelson, M. J., Que, L. Jr., and Wallick, D. E. (1988) Catecholate LMCT bands as probes for the active sites of nonheme iron oxygenases. *J. Am. Chem. Soc. 110*, 2026−2032.

(29) Anitha, N., and Palaniandavar, M. (2011) Mononuclear iron(III) complexes of 3N ligands in organized assemblies: Spectral and redox properties and attainment of regioselective extradiol dioxygenase activity. *J. Chem. Soc., Dalton Trans. 40*, 1888−1901.

(30) Stallings, M. D., Morrison, M. M., and Sawyer, D. T. (1981) Redox chemistry of metal-catechol complexes in aprotic media. 1. Electrochemistry of substituted catechols and their oxidation products. *Inorg. Chem. 20*, 2655−2660.

(31) Chedekel, M. R., Land, E. J., Thompson, A., and Truscott, T. G. (1984) Early steps in the free radical polymerization of 3,4-dihydroxyphenylalanine (dopa) into melanin. *J. Chem. Soc., Chem. Commun.,* 1170−1172.

(32) Hartl, F., Stufkens, D. J., and Vlcek, A. Jr. (1992) Nature of the manganese(I)-dioxolene bonding as a function of the ligand oxidation state: UV-visible, IR, and resonance Raman spectroelectrochemical study of $[Mn(CO)_3L_n(Diox)]^z$ (n = 0, 1; z = −2, −1, 0, +1) and $[Mn(CO)_2\{P(OEt)_3\}_m(Diox)]^z$ (m = 1, 2; z = −1, 0, +1) complexes. *Inorg. Chem. 31*, 1687−1695.

(33) Mialane, P., Anxolabeheremallart, E., Blondin, G., Nivorojkine, A., Guilhem, J., Tchertanova, L., Cesario, M., Ravi, N., Bominaar, E., Girerd, J. J., and Münck, E. (1997) Structure and electronic properties of (N,N′-Bis(4-Methyl-6-Tert-Butyl-2-Methyl-Phenolate)-N,N′-bis-methyl-1,2-di aminoethane)Fe-III (DBSQ): Spectroelectrochemical study of the red-ox properties. Relevance to intradiol catechol dioxygenases. *Inorg. Chim. Acta 263*, 367−378.

(34) Kessel, S. L., Emberson, R. M., Debrunner, P. G., and Hendrickson, D. N. (1980) Iron(III), manganese(III), and cobalt(III) complexes with single chelating o-semiquinone ligands. *Inorg. Chem. 19*, 1170−1178.

(35) Lynch, M. W., Valentine, M., and Hendrickson, D. N. (1982) Mixed-valence semi-quinone catecholate iron complexes. *J. Am. Chem. Soc. 104*, 6982−6989.

(36) Siegbahn, P. E. M., and Haeffner, F. (2004) Mechanism for catechol ring-cleavage by non-heme iron extradiol dioxygenases. *J. Am. Chem. Soc. 126*, 8919−8932.

(37) Deeth, R. J., and Bugg, T. D. H. (2003) A density functional investigation of the extradiol cleavage mechanism in non-heme iron catechol dioxygenases. *J. Biol. Inorg. Chem. 8*, 409−418.
(38) Girerd, J.-J., Banse, F., and Simaan, A. J. (2000) Characterization and properties of non-heme iron peroxo complexes. *Struct. Bonding (Berlin, Ger.) 97*, 145−177.
(39) Roelfes, G., Vrajmasu, V., Chen, K., Ho, R. Y., Rohde, J.-U., Zondervan, C., La Crois, R. M., Schudde, E. P., Lutz, M., Spek, A. L., Hage, R., Feringa, B. L., Münck, E., and Que, L. Jr. (2003) End-on and side-on peroxo derivatives of non-heme iron complexes with pentadentate ligands: models for putative intermediates in biological iron/dioxygen chemistry. *Inorg. Chem. 42*, 2639−2653.
(40) Karlsson, A., Parales, J. V., Parales, R. E., Gibson, D. T., Eklund, H., and Ramaswamy, S. (2003) Crystal structure of naphthalene dioxygenase: Side-on binding of dioxygen to iron. *Science 299*, 1039−1042.
(41) Neibergall, M. B., Stubna, A., Mekmouche, Y., Münck, E., and Lipscomb, J. D. (2007) Hydrogen peroxide dependent cis-dihydroxylation of benzoate by fully oxidized benzoate 1,2-dioxygenase. *Biochemistry 46*, 8004−8016.